



with a resolution of  $48 \times 33 \times 48$  modes subject to periodic boundary conditions in the homogeneous directions and enforced shift-and-reflect symmetry  $(u, v, w)[x, y, z] \equiv \sigma_{SR}(u, v, w)[x, y, z] = (u, v, -w)[x + L_x/2, y, -z]$ .

Plane Couette flow is linearly stable for all  $Re$  and the first (known) non-trivial invariant solutions are the Nagata-Busse-Clever (NBC) states [25, 27, 28], a pair of fixed points that are created in a saddle-node bifurcation. In our domain the bifurcation takes place at  $Re = 163.8$  and the upper-branch solution (with higher energy) is attracting while the lower branch has a single unstable direction. As a consequence, its stable manifold forms the separating boundary between trajectories approaching the upper branch and the laminar state [29, 30]. Increasing  $Re$ , the upper branch undergoes a period doubling cascade, generating chaos. At  $Re = 188.51$  the chaotic attractor formed around the upper branch subsequently collides with the lower branch. In this boundary crisis [6], the chaotic attractor becomes “leaky” and turns into a chaotic saddle, from which trajectories eventually escape. Similar scenarios have been found for periodic [31] and localized [32] structures in pipe flow as well as in magnetohydrodynamics [33], indicating a generic mechanism by which the saddle that supports first short-lived turbulent transients in shear flows is created. Similar scenarios are well-known in low-dimensional dynamical systems [34–36].

As  $Re$  increases, the chaotic saddle grows to fill a larger part of state space. In Fig. 1 this is visualized for three successively increasing  $Re$  by plotting the lifetimes of initial conditions, see figure caption for details. Blue regions correspond to initial conditions that directly laminarize while the chaotic saddle appears as colorful fractal regions of rapidly varying lifetimes indicative of the sensitive dependence on initial condition. Since the lower branch solution has a single unstable direction, its stable manifold is of co-dimension one and the general topology of state space can be understood in a two-dimensional section. For  $Re=210$  (panel *a*), the saddle only occupies a small area. As  $Re$  increases (panels *b* and *c*), the colorful fractal regions marking the saddle both grow and the variations inside become denser. As expected, the survival probabilities, shown in panel *d*, show exponential tails indicating a constant escape probability from the saddle. Their slope, the characteristic lifetime  $\tau$ , increases with  $Re$  as the saddle structure fills the domain.

How does the complexity of the saddle increase? We explore one mechanism and specifically demonstrate a sequence of bifurcation events, in which an infinite number of invariant solutions is added to the saddle, leading to an increase in lifetimes; the mechanism bears a strong resemblance with the events at the creation of the saddle as summarized above. At  $Re = 249.01$  a local saddle-node bifurcation creates a pair of new solutions which are not fixed points as the NBC-states but periodic orbits of period  $T \simeq 60$ . Of those, as for the NBC-states,

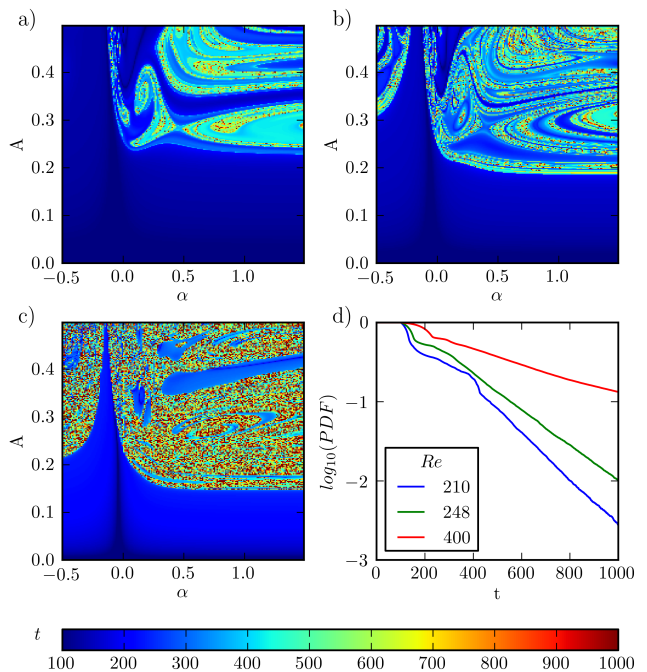


FIG. 1. (color online) (a) - (c): The growing turbulent saddle in state space for different Reynolds numbers, visualized by the lifetime of initial conditions in a 2D section. The 50,000 initial conditions in each panel are chosen by interpolating between lower- and upper-branch NBC-solutions on the x-axis and rescaling the perturbation amplitude  $A$  on the y-axis. The x-axis is rescaled such that the  $L_2$ -distance of the NBC-states is proportional to their distance in the projection, giving a physical meaning to the scales in the figure:  $u = Au_\alpha/\|u_\alpha\|$ ,  $u_\alpha = u_{LB} + \alpha(u_{UB} - u_{LB})/\sqrt{\|u_{UB} - u_{LB}\|^2 - (\|u_{UB}\| - \|u_{LB}\|)^2}$ ; In the sequence a)  $Re = 210$ . b)  $Re = 248$ . c)  $Re = 400$ , the saddle grows while it develops ever finer striations, indicating the structures supporting the saddle to get denser. d) Survival probabilities for the presented Reynolds numbers show clear exponential tails with increasing slope, indicating a characteristic lifetime which increases with  $Re$ .

the lower branch has a single unstable direction and the upper branch solution is an attractor. The stable periodic orbit is surrounded by its basin of attraction, visible in Fig. 2b) at  $Re = 249.1$ . As  $Re$  increases, the orbit undergoes a bifurcation cascade, creating infinitely many invariant states and generating a local chaotic attractor (panel c). On further increasing  $Re$ , the chaotic attractor grows until at  $Re_c = 250.13$  it collides with its own basin boundary in a crisis bifurcation. While the signature of the basin of attraction of the former attractor is still visible for  $Re > Re_c$  (panel d), trajectories may now escape from the newly created “inner” saddle into the already existing “outer” one. Thus at the crisis bifurcation the infinitely many invariant solutions from the former chaotic attractor are added to the turbulent saddle. As before, the two-dimensional visualization captures the essential

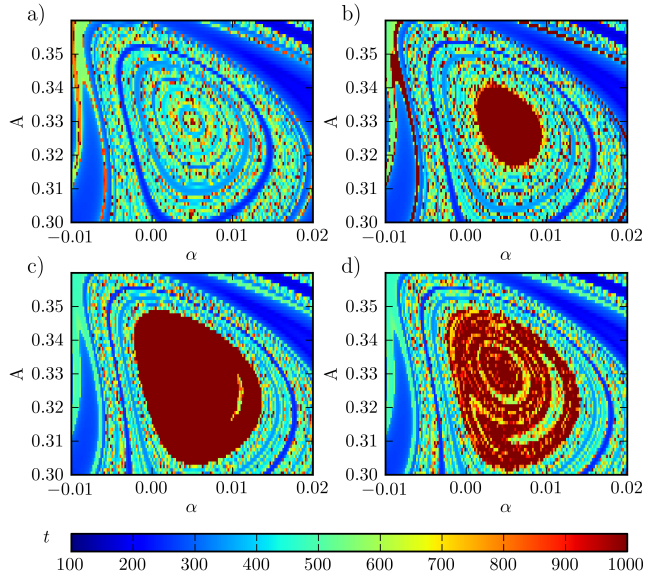


FIG. 2. (color online) Growth of the turbulent saddle via the emergence of a chaotic attractor followed by its destruction in a boundary crisis. Visualized is a small region of the saddle in a projection similar to Fig. 1 but spanned by the new pair of periodic orbits at  $Re = 250$  (with the phase such that energy is maximal.) Within the pre-existing chaotic saddle at  $Re = 248.5$  (a) the saddle-node bifurcation creates the new pair of two periodic orbits, of which one is stable. Its basin of attraction at  $Re = 249.1$  (b) just after the bifurcation is visible as the red region of initial conditions that never reach the laminar state. On further increasing  $Re$ , the orbit undergoes a bifurcation cascade generating a chaotic attractor, shown at  $Re = 250.1$  (c), whose basin of attraction has grown. At  $Re_c = 250.13$  the attractor collides with its boundary in a crisis bifurcation. Beyond the crisis bifurcation, the attractor has turned into a repeller and it is now a part of the turbulent saddle. The remnant of the attractor’s basin of attraction remains visible at  $Re = 250.25$  (d), where now the new “inner” saddle is immersed in the “outer” one.

features of the process since the lower-branch orbit has only a single unstable direction and hence a stable manifold of co-dimension one.

Over the sequence of these bifurcations, the decay rate from the turbulent saddle to the laminar state varies non-monotonically. Before the saddle-node bifurcation at  $Re = 249.01$ , the survival probabilities are distributed exponentially (Fig. 3a). Beyond  $Re = 249.01$ , there are initial conditions that are trapped inside the stable region and never decay. Thus, the overall distribution is a linear superposition of an exponential and a constant. The contribution of the non-decaying trajectories increases with higher Reynolds numbers as the attractor grows to fill more of the projection plane. After the boundary crisis at  $Re = 250.13$ , the new bubble becomes a part of the turbulent saddle. Initially the escape rate from the newly created embedded part of the saddle differs substantially from the outer saddle’s escape rate. Thus, for

short observation times the distribution is a linear superposition of two different exponentials resulting in a non-exponential variation.

To quantify the variation of lifetimes due to both parts of the saddle, we separate initial conditions into two groups corresponding to the location of the former attractor in the discussed projection plane and compute lifetimes for both parts of the saddle independently. This is detailed for  $Re = 250.25$  in Fig. 3c, where instead of a *normalized* survival probability we plot the absolute number of initial conditions that survive for a given time. Since the initial conditions are uniformly distributed over the area shown in Fig. 2 the absolute numbers are a measure of the state space area that contributes to a given lifetime. The total number of data points is separated into those initial conditions from the inner and outer saddle. In Fig. 3 both individual distributions show clear exponential tails with characteristic lifetimes of 700 and 180, respectively. The sum of the two exponentials, weighted by the number of initial conditions in the two regions, (thick black line) almost perfectly recovers the total distribution. Similar non-exponential distributions due to several weakly connected saddle structures have also been studied in Hamiltonian systems, where nested saddles are shown to generate algebraic lifetime distributions [37].

The variation of  $\tau$  with  $Re$  for both the inner and outer saddle region is shown in Fig. 3(b). While it remains almost constant for the outer region, in the inner region the lifetime diverges while the attractor exists and drops after the boundary crisis, well approximated by a power law with exponent  $-2.1$ . The characteristic lifetime levels off slightly above the value of the outer saddle, indicating that trajectories that leave the inner saddle have to first pass through the outer one before decaying. Consequently, those trajectories have longer lifetimes. At higher  $Re$ , additional heteroclinic bifurcations will enhance the dynamical connectivity between the inner and outer saddle region which finally translates the higher lifetimes from the inner region to the whole saddle. Thereby, the characteristic lifetime of the saddle increases when it expands due to the incorporation of the newly created turbulent bubble.

We have found sudden expansions of the structure of the chaotic saddle at discrete Reynolds numbers as discussed for  $Re \simeq 250$  at various  $Re$ , indicating that the mechanism is a generic way to increase the complexity of the state space. While the presented example of a *stable* periodic orbit emerging in a saddle-node bifurcation followed by a chaotic cascade and a boundary crisis of a transiently existing attractor is observed for many parameters in our system, a more general variant of the discussed mechanism starts with *unstable* states. The sequence of events described above then appears in a weakly unstable subspace of the full system. This does not involve a global attractor for intermediate  $Re$  and

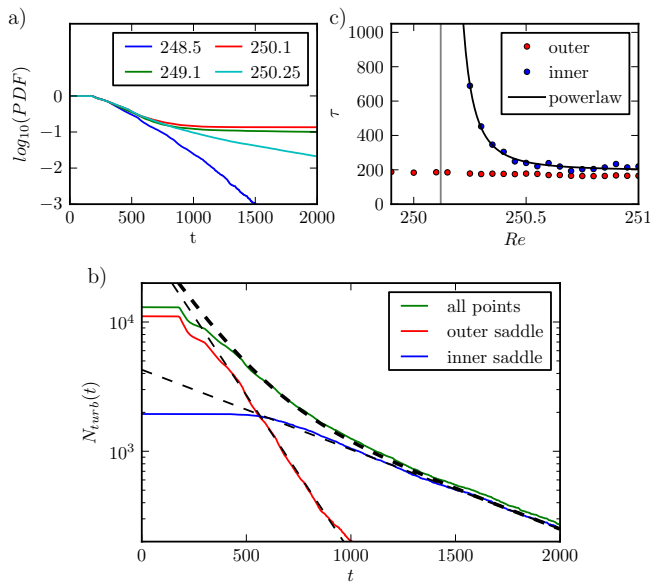


FIG. 3. (color online) Variations of lifetimes with Reynolds number. (a) Survival probability calculated from the data in Fig. 2 for all four  $Re$ . Before the saddle-node bifurcation ( $Re = 248.5$ ), survival probabilities are exponentially distributed. After the bifurcation, the attractor causes an offset corresponding to the initial conditions that never decay. After the boundary crisis ( $Re=250.25$ ), the distribution is non-exponential. b) Detailed analysis of the lifetime statistics at  $Re = 250.25$ , with the total number of trajectories that have not decayed up to a given time  $t$  as a function of time. In Fig. 2d the shape of the former attractor is still visible and allows to calculate the characteristic lifetime separately for initial conditions from the new, inner saddle and the outer saddle. Both show exponential tails with a characteristic lifetime of 700 and 180, respectively. The thick dashed line on top shows the weighted average of the two exponentials – it perfectly fits the actual distribution apart from the trajectories that decay immediately. c) Reynolds number vs. characteristic lifetime  $\tau$  as a function of  $Re$ , calculated separately for initial conditions from the inner and outer saddle. Lifetimes from the outer saddle are almost constant. For the data from the inner saddle, it is infinite up to the point of the crisis bifurcation, after which it drops drastically with a power-law behavior and levels slightly above the value of the outer saddle, showing that lifetimes have increased.

is hence more difficult to detect as the lifetimes do not diverge. Yet, the same scenario still increases the complexity of the saddle, leading to growing lifetimes.

The formation of turbulent bubbles and their destruction at discrete  $Re$  values constitutes abrupt changes in the state space of shear flows. The described mechanism naturally leads to non-smooth and non-monotonic variations of  $\tau$  as well as non-exponential lifetime statistics. While we have found these features for intermediate  $Re$  in the considered system they have not been reported yet for experimental lifetime studies. Apart from the symmetry restriction, which is only possible in numerics, one challenge is that the bifurcations become dense in  $Re$  and

begin to overlap. To resolve this, very fine steps in  $Re$  are needed, as well as a very exact control of the applied perturbation. In a sufficiently coarse grained analysis, an apparent smooth variation emerges due to the collective effect of many bifurcations.

The mechanism we explored in this letter allows to directly relate state-space structures and their variation to statistical properties of transitional flows. While our analysis is focused on plane Couette flow, recent investigations of pipe flow and even magnetohydrodynamic systems suggest that the described mechanism by which turbulent saddles grow in complexity are very generic. This emphasizes the significance of low-dimensional dynamical systems theory for understanding the physics of fluid mechanical systems with a subcritical transition to turbulence.

- 
- [1] S. Grossmann, *Rev. Mod. Phys.* **72**, 603 (2000).
  - [2] A. G. Darbyshire and T. Mullin, *J. Fluid Mech.* **289**, 83 (1995).
  - [3] A. Schmieguel and B. Eckhardt, *Phys. Rev. Lett.* **79**, 5250 (1997).
  - [4] B. Eckhardt, T. M. Schneider, B. Hof, and J. Westerweel, *Annu. Rev. Fluid Mech.* **39**, 447 (2007).
  - [5] B. Eckhardt, *Nonlinearity* **21**, T1 (2008).
  - [6] T. Kreilos and B. Eckhardt, *Chaos* **22**, 047505 (2012).
  - [7] G. Kawahara, M. Uhlmann, and L. van Veen, *Annu. Rev. Fluid Mech.* **44**, 203 (2012).
  - [8] C. Grebogi, E. Ott, and J. A. Yorke, *Phys. Rev. Lett.* **57**, 1284 (1986).
  - [9] S. Bottin and H. Chaté, *Eur. Phys. J. B* **6**, 143 (1998).
  - [10] B. Hof, J. Westerweel, T. M. Schneider, and B. Eckhardt, *Nature* **443**, 59 (2006).
  - [11] J. Peixinho and T. Mullin, *Phys. Rev. Lett.* **96**, 094501 (2006).
  - [12] A. P. Willis and R. R. Kerswell, *Phys. Rev. Lett.* **98**, 014501 (2007).
  - [13] B. Hof, A. de Lozar, D. J. Kuik, and J. Westerweel, *Phys. Rev. Lett.* **101**, 214501 (2008).
  - [14] T. M. Schneider and B. Eckhardt, *Phys. Rev. E* **78**, 046310 (2008).
  - [15] T. M. Schneider, F. De Lillo, J. Buehrle, B. Eckhardt, T. Dörnemann, K. Dörnemann, and B. Freisleben, *Phys. Rev. E* **81**, 015301(R) (2010).
  - [16] R. R. Kerswell, *Nonlinearity* **18**, R17 (2005).
  - [17] J. P. Crutchfield and K. Kaneko, *Phys. Rev. Lett.* **60**, 2715 (1988).
  - [18] L. P. Kadanoff and C. Tang, *Proc. Natl. Acad. Sci. U. S. A.* **81**, 1276 (1984).
  - [19] Y. Duguet, a. P. Willis, and R. R. Kerswell, *J. Fluid Mech.* **613**, 255 (2008).
  - [20] J. F. Gibson, J. Halcrow, and P. Cvitanović, *J. Fluid Mech.* **611**, 107 (2008).
  - [21] J. Vollmer, T. M. Schneider, and B. Eckhardt, *New J. Phys.* **11**, 1 (2009), NoStop
  - [22] L. van Veen and G. Kawahara, *Phys. Rev. Lett.* **107**, 114501 (2011).
  - [23] K. T. Allhoff and B. Eckhardt, *Fluid Dyn. Res.* **44**,

- 031201 (2012).
- [24] K. Avila, D. Moxey, A. de Lozar, M. Avila, D. Barkley, and B. Hof, *Science* **333**, 192 (2011).
- [25] F. Waleffe, *Phys. Rev. Lett.* **81**, 4140 (1998).
- [26] J. F. Gibson, *Channelflow: A spectral Navier-Stokes simulator in C++*, Tech. Rep. (U. New Hampshire, 2012).
- [27] M. Nagata, *J. Fluid Mech.* **217**, 519 (1990).
- [28] R. M. Clever and F. H. Busse, *J. Fluid Mech.* **344**, 137 (1997).
- [29] J. D. Skufca, J. A. Yorke, and B. Eckhardt, *Phys. Rev. Lett.* **96**, 174101 (2006).
- [30] T. M. Schneider, J. F. Gibson, M. Lagha, F. De Lillo, and B. Eckhardt, *Phys. Rev. E* **78**, 037301 (2008).
- [31] F. Mellibovsky and B. Eckhardt, *J. Fluid Mech.* **709**, 149 (2012), NoStop
- [32] M. Avila, F. Mellibovsky, N. Roland, and B. Hof, *Phys. Rev. Lett.* **110**, 224502 (2013).
- [33] A. Riols, F. Rincon, C. Cossu, G. Lesur, P.-Y. Longaretti, G. I. Ogilvie, and J. Haurault, *J. Fluid Mech.* **731**, 1 (2013), NoStop
- [34] C. Grebogi, E. Ott, and J. A. Yorke, *Physica D* **7**, 181 (1983).
- [35] Y.-C. Lai and C. Grebogi, *Phys. Rev. E* **49**, 1094 (1994).
- [36] Y.-C. Lai and T. Tél, *Transient Chaos: Complex Dynamics on Finite Time Scales* (Springer, 2011).
- [37] J. D. Hanson, J. R. Cary, and J. D. Meiss, *J. Stat. Phys.* **39**, 327 (1985).